βIV spectrin is recruited to axon initial segments and nodes of Ranvier by ankyrinG

Yang Yang, Yasuhiro Ogawa, Kristian L. Hedstrom, and Matthew N. Rasband

Department of Neuroscience, University of Connecticut Health Center, University of Connecticut, Farmington, CT 06032

High densities of ion channels at axon initial segments (AISs) and nodes of Ranvier are required for initiation, propagation, and modulation of action potentials in axons. The organization of these membrane domains depends on a specialized cytoskeleton consisting of two submembranous cytoskeletal and scaffolding proteins, ankyrinG (ankG) and βIV spectrin. However, it is not known which of these proteins is the principal organizer, or if the mechanisms governing formation of the cytoskeleton at the AIS also apply to nodes. We identify a distinct protein domain in βIV spectrin required for its localization to the AIS, and show that this domain mediates βIV spectrin's interaction with ankG. Dominant-negative ankG disrupts βIV spectrin localization, but does not alter endogenous ankG or Na^+ channel clustering at the AIS. Finally, using adenovirus for transgene delivery into myelinated neurons, we demonstrate that βIV spectrin recruitment to nodes of Ranvier also depends on binding to ankG.

Introduction

Neurons are highly polarized cells with morphologically and functionally distinct subcellular domains. The axon initial segment (AIS) and node of Ranvier are two axonal domains characterized by an "electron-dense" membrane undercoating consisting of voltage-gated Na^+ and K^+ channels (Nav and Kv, respectively), cell adhesion molecules (CAMs), and a specialized membrane cytoskeleton (Poliak and Peles, 2003; Salzer, 2003). These domains act as the generator for action potential initiation and propagation (Khaliq and Raman, 2006; Naundorf et al., 2006), and the diffusion barrier for maintaining axonal polarity (Winckler et al., 1999). Disruption of these membrane domains or their molecular composition contributes to the pathophysiology of many nervous system diseases, including epilepsy, multiple sclerosis, and spinal cord injury (Chen et al., 2004; Craner et al., 2004; Sasaki et al., 2006). Consequently, any therapeutic strategy aimed at treating these diseases and reversing their devastating effects will require a detailed understanding of the mechanisms responsible for node and AIS formation and maintenance.

From both molecular and functional standpoints, the AIS and nodes of Ranvier are very similar; they have nearly every protein component in common, and both provide the ionic currents necessary for membrane depolarization and action potential initiation/propagation. Despite these strong similarities, one major difference between these two membrane domains is that node formation requires myelination by Schwann cells or oligodendrocytes, but the AIS is intrinsically organized by the neuron. Thus, nodes form "outside-in," whereas the AIS forms "inside-out" (for review see Hedstrom and Rasband, 2006).

The ankyrin and spectrin protein families play important roles in regulating protein localization and membrane domain formation in many different cell types (Bennett and Baines, 2001). For example, in erythrocytes the spectrin-based membrane skeleton is essential for maintaining the cell's biconcave shape and restricting the lateral mobility of the anion exchanger through the scaffolding protein ankyrinR (ankR; Delaunay, 2006). The identification and localization of neuronal ankyrinG (ankG) and βIV spectrin provided important clues for the mechanism of AIS and node formation in axons (Kordeli et al., 1995; Berghs et al., 2000). During development, both ankG and βIV spectrin define putative nodes and initial segments before ion channels cluster (Rasband et al., 1999; Jenkins and Bennett, 2001). In a mouse lacking ankG in Purkinje neurons, Nav and KCNQ2/3 Kv channels, neurofascin-186, and βIV spectrin all fail to cluster at the AIS (Zhou et al., 1998; Jenkins and Bennett, 2001; Komada and Soriano, 2002; Pan et al., 2006). Further, distinct protein domains in Nav channels, KCNQ2/3 Kv channels, and NF-186 have been identified that mediate their interactions with ankG (Garver et al., 1997; Garrido et al., 2003; Lemaillet et al., 2003; Pan et al., 2006). Together, these results all point to ankG as a principal organizer of the membrane proteins located at the AIS. However, in mice lacking βIV spectrin,

Correspondence to Matthew N. Rasband: Rasband@uchc.edu

Abbreviations used in this paper: AIS, axon initial segment; CAM, cell adhesion molecule; CNS, central nervous system; DIV, days in vitro; DRG, dorsal root ganglion; E, embryonic day; PNS, peripheral nervous system; RGC, retinal ganglion cell.

The online version of this article contains supplemental material.

The Journal of Cell Biology, Vol. 176, No. 4, February 12, 2007 509–519
http://www.jcb.org/cgi/doi/10.1083/jcb.200610128

neither ankG nor Nav channels correctly localize to the AIS, indicating that like ankG, βIV spectrin is also indispensable for domain organization (Komada and Soriano, 2002). To determine whether βIV spectrin directs the formation of the AIS and nodes of Ranvier, we identified the molecular mechanisms regulating its recruitment to these domains.

Results

Throughout the central nervous system, AISs are characterized by high densities of Nav channels that colocalize with ankG (Fig. 1 A; Jenkins and Bennett, 2001; Boiko et al., 2003). Despite large dendrites and long axons, high densities of Nav channels and ankG are only found in short ∼20–40-μm-long domains at the proximal region of the axon adjacent to the cell body (Fig. 1 A). To determine how this specificity is achieved, we used the well-characterized embryonic hippocampal neuron culture system (Banker and Goslin, 1998) to study the molecular mechanisms regulating AIS formation; this model has been used previously to elucidate the mechanisms regulating protein sorting and targeting in neurons (Lim et al., 2000; Silverman et al., 2001; Sampo et al., 2003; Wisco et al., 2003; Lee et al., 2004).

To determine if cultured hippocampal neurons form an AIS, we immunostained these neurons after 7–10 d in vitro (DIV) using antibodies against Nav channels, βIV spectrin, and ankG; antibodies against MAP2 were used to identify somatodendritic domains. These neurons typically had 1–2 axons that could be distinguished from dendrites by the enrichment for AIS proteins at the proximal region of the axon adjacent to the cell soma and the absence of MAP2 staining (Fig. 1, B and C). There was a marked increase in AIS proteins that corresponded to a complementary decrease in MAP2 (Fig. 1, B and C, fluorescence intensity profiles). Thus, hippocampal neurons in vitro form well-defined initial segments that are molecularly identical to those observed in vivo.

Characterization of AIS formation in vitro

To determine the time course of AIS formation in vitro, we immunostained neurons at different developmental stages (1–7, 14, and 21 DIV) using antibodies against Nav channels. We found that the percentage of neurons with an AIS defined by Nav channel staining increased dramatically during the first week (Fig. 1, D–F). At 1 DIV, only 14 ± 3% of neurons had AIS Nav channel immunoreactivity, but this percentage increased to 94 ± 2% at 7 DIV, and included 100% of neurons by 14 DIV (Fig. 1 E; typical Nav channel staining of hippocampal neurons at three time points is shown in Fig. 1 D). Fluorescence intensity profiles along the axon as a function of DIV showed that the density of Nav channels continued to increase at the AIS from 7 to 21 DIV (Fig. 1 F). These results also demonstrate that axon specification precedes recruitment of Nav channels to the AIS (Banker and Goslin, 1998).

Spectrin repeat 15 is essential for localization of βIV spectrin to the AIS

How is βIV spectrin localized at the AIS? βIV spectrin undergoes extensive alternative splicing with at least six different variants (Berghs et al., 2000; Komada and Soriano, 2002). Among these, the βIVΣ1 and βIVΣ6 splice variants are both located at nodes of Ranvier and the AIS (Lacas-Gervais et al., 2004). βIVΣ1 consists of an N-terminal actin-binding domain followed by 17 spectrin repeats, a specific domain that is unique among the β-spectrins, and a C-terminal pleckstrin homology domain; βIVΣ6 is identical to the C-terminal half of βIVΣ1 (Fig. 2 A). Because βIVΣ6 is located at nodes and the AIS in a mouse lacking βIVΣ1 (Lacas-Gervais et al., 2004), we reasoned that the AIS localization determinant must be distal to the 10th spectrin repeat (SR10). To test this possibility, we first introduced Myc-tagged βIVΣ6 (Myc-βIVΣ6) into cultured hippocampal neurons at 7 DIV because initial segments, which were defined by Nav channel immunostaining, can be detected in most neurons at this time (Fig. 1 E). 1 d later, Myc immunoreactivity (red) was detected at the AIS in a pattern identical to that of endogenous βIV spectrin (Fig. 2, B and C).

Because the restricted localization of Myc-βIVΣ6 at the AIS of cultured hippocampal neurons provides a very simple functional assay, we undertook a deletion strategy to identify the protein domain necessary for βIV spectrin localization. We generated a series of progressively shorter Myc-βIVΣ6 mutants by introducing a premature stop codon (Fig. 2 A) between spectrin repeats. In the case of the Myc–"*quivering 3J*" (qv^{3J}) mutant construct, we introduced the same point mutation as found in the qv^{3J} mouse (Parkinson et al., 2001; Yang et al., 2004). Transient transfection of these plasmids into CHO cells, followed by immunoblotting with Myc antibodies, shows that all mutants are expressed at the expected molecular weights (Fig. S1 A, available at http://www.jcb.org/cgi/content/full/jcb.200610128/DC1).

To determine which of the mutant Myc-βIV spectrin proteins retain the capacity to localize at the AIS, we transfected each construct into hippocampal neurons at 7 DIV and immunostained these neurons for MAP2 and Myc immunoreactivity 1 d later. As with full-length Myc-βIVΣ6 (Fig. 2 B), >80% of the Myc-qv^{3J}–(Fig. S1 B) and Myc-SR10-15–transfected (Fig. 2 D) neurons had Myc immunoreactivity at the AIS (Fig. 2 D, red, arrow). In contrast, βIV spectrin proteins lacking SR15 (Fig. 2 E, Myc-SR10-14; Fig. S1 C, Myc-SR10-13; and Fig. S1 D, Myc-SR10-11) all failed to localize at the AIS (arrows). In these transfected neurons, Myc immunoreactivity along the axon corresponded closely to that of MAP2 (see the fluorescence intensity profiles at right).

Based on the aforementioned truncation analysis, we conclude that SR15 is essential for proper AIS localization. To test this more directly, we generated a short, Myc-tagged βIV spectrin protein consisting of only SR14-15 (Myc-SR14-15; Fig. 2 A). When transfected into neurons, this protein could be detected at the AIS (Fig. 2 F, arrow). However, it was also more enriched in the soma than Myc-βIVΣ6, Myc-qv^{3J}, or Myc-SR10-15. Collectively, these results strongly suggest that SR15 is required for the localization of βIV spectrin to the AIS.

Spectrin repeat 15 of βIV spectrin interacts specifically with ankG

What is the molecular basis for SR15-dependent targeting of βIV spectrin to the AIS? Previous studies of ion channels and

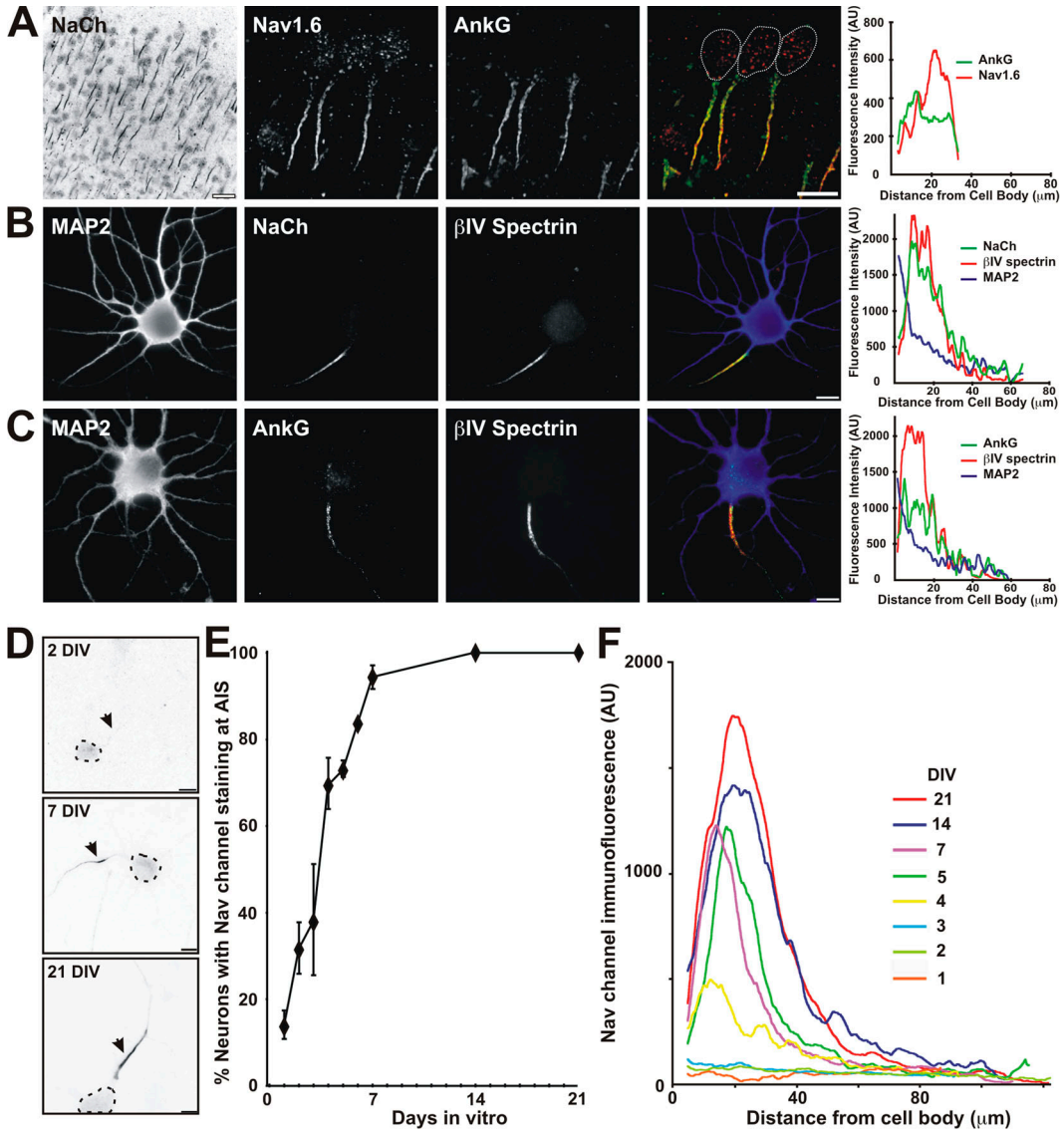

Figure 1. **Hippocampal neurons have a well-defined AIS both in vivo and in vitro.** (A, left) Low magnification view of rat cortex immunostained for Nav channels (NaCh). (right) Higher magnification view of cortical neurons immunostained for Nav1.6 (red) and ankG (green). Cell bodies are outlined with dotted lines. (B) Nav channels (green) and βIV spectrin (red) are clustered in the AIS of a 10 DIV hippocampal neuron. MAP2 (blue) labels the cell soma and dendrites. (C) AnkG (green) and βIV spectrin (red) are clustered in the AIS of a 7 DIV hippocampal neuron. MAP2 (blue) labels the cell soma and dendrites. (D) Cultured hippocampal neurons at different developmental stages (2, 7, and 21 DIV) showed gradual accumulation of Nav channels at the AIS (arrows). Cell bodies are indicated by the dotted lines. (E) The formation of the AIS was measured by the percentage of neurons with Nav channels clustered at the AIS in MAP2-positive neurons during development (n = 200 neurons at each time point, in three independent experiments). Error bars represent the mean ± the SD. (F) AIS Nav channel immunofluorescence intensity was measured during the first 3 wk in culture. Each line represents the average intensity from 10 neurons at each developmental time point. In A–C, immunofluorescence intensities along axons are shown at the right of each image. AU, arbitrary units. Bars: (A, left) 25 μm; (A, right, and B–D) 10 μm.

CAMs restricted to the AIS have shown that their localization depends on binding to ankG (Garrido et al., 2003; Lemaillet et al., 2003; Pan et al., 2006), and ankG-null neurons lack βIV spectrin at their AIS (Komada and Soriano, 2002). Further, in vitro binding assays suggested that erythrocyte ankyrin (ankR) binds to SR15 of erythrocyte β-spectrin (Kennedy et al., 1991). Therefore, we considered the possibility that βIVSR15 might interact with ankG, and that this interaction might be the basis for the localization of βIV spectrin at the AIS. To test this, Myc-βIVΣ6 or mutant constructs (Fig. 2 A) were cotransfected into CHO cells together with a GFP-tagged 270-kD splice variant of ankG (AnkG-GFP; ankG is found in both 270- and 480-kD splice variants at the AIS and nodes of Ranvier; Zhang and Bennett, 1998). We immunoprecipitated AnkG-GFP, and then determined if Myc-tagged βIV spectrin proteins were co-immunoprecipitated. Immunoblots of these immunoprecipitation reactions demonstrated that all proteins containing SR15 (Myc-βIVΣ6, Myc-qv^{3J}, Myc-SR10-15, and Myc-SR14-15) coimmunoprecipitated with AnkG-GFP (Fig. 3 A). However, proteins lacking SR15 (Myc-SR10-14, Myc-SR10-13, and Myc-SR10-11) failed to coimmunoprecipitate with AnkG-GFP. AnkG-GFP was detected in all anti-GFP immunoprecipitations (unpublished data).

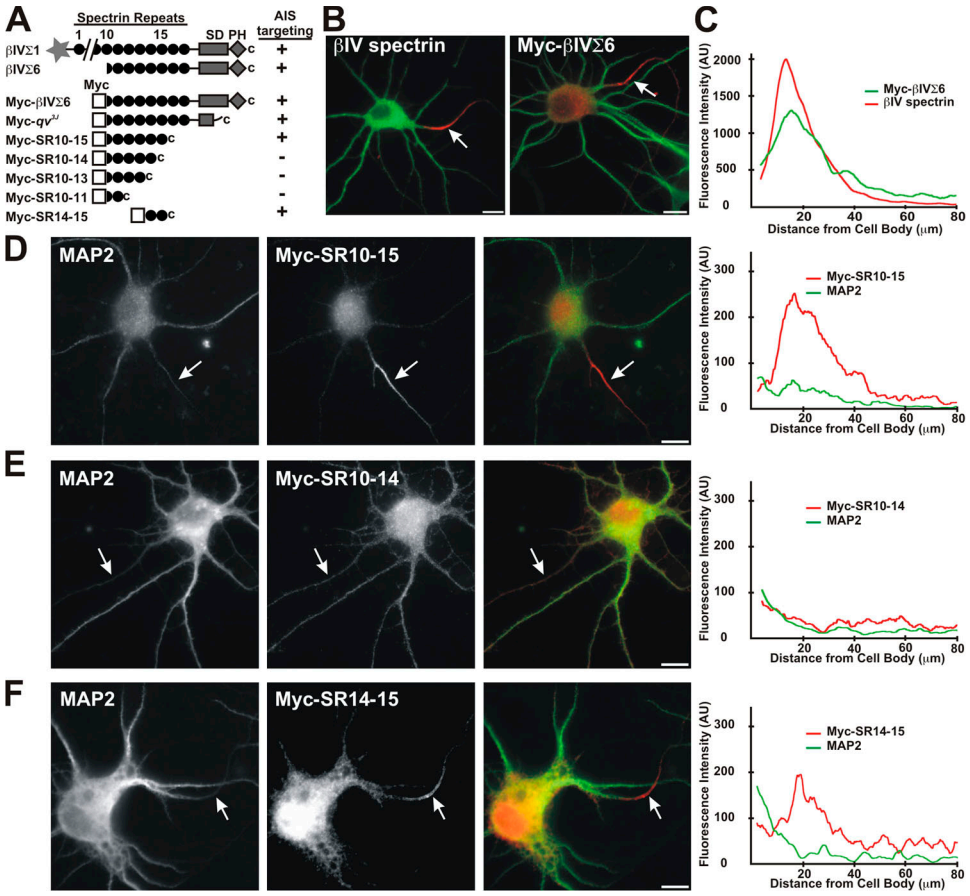

Figure 2. **AIS Localization of βIV spectrin requires the 15th spectrin repeat.** (A) Domain structure of βIV spectrin and Myc-βIVΣ6 spectrin constructs. All constructs were Myc-tagged at the N terminus. Whether each protein is located at the AIS in brain or in cultured hippocampal neurons is indicated. In B–F, the somatodendritic domain is defined by MAP2 immunoreactivity (green). (B) Endogenous βIV spectrin (red) is located at the AIS of a 7 DIV hippocampal neuron. Similarly, introduced Myc-βIVΣ6 spectrin (red) is also restricted to the AIS. (C) Fluorescence intensity profiles show that both endogenous (red) and introduced (Myc-βIVΣ6; green) βIV spectrin localize at the AIS. Profiles are averages from 20 neurons. (D) Myc-SR10-15 is located at the AIS (red, arrows). (E) Myc-SR10-14 fails to cluster at the AIS and is located throughout the somatodendritic domain. The axon is indicated by an arrow. (F) Myc-SR14-15 is located at the AIS (red, arrows) and in the soma of the cell. In D–F, fluorescence intensity profiles along each axon for Myc (red) and MAP2 (green) immunoreactivity are shown on the far right. Bars, 10 μm.

These results suggest that SR15 of βIV spectrin is required for binding to ankG, and that the AIS localization of βIV spectrin depends on binding to ankG.

Because hippocampal neurons also express ankyrinB (ankB) and other β spectrins, including βI, βII, and βIII spectrin (Fig. S1 E; Leshchyns'ka et al., 2003; Ogawa et al., 2006), we tested the specificity of the ankG–βIV spectrin interaction. We cotransfected Myc-βIVΣ6 and a GFP-tagged ankB (AnkB-GFP) or AnkG-GFP. However, although more AnkB-GFP was immunoprecipitated compared with AnkG-GFP, we were unable to detect any interaction between AnkB-GFP and Myc-βIVΣ6 (Fig. 3 B). We also cotransfected AnkG-GFP together with a GFP-tagged βIII spectrin (βIII-GFP), immunoprecipitated AnkG-GFP using anti-ankG, and immunoblotted the immunoprecipitate using anti-βIII spectrin. However, we were unable to detect any βIII-GFP in the immunoprecipitate (Fig. 3 B, IP). These results are consistent with the fact that neither ankB nor βIII spectrin are located at the AIS of hippocampal neurons (Fig. S1 E; Ogawa et al., 2006). Thus, the interaction between ankG and βIV spectrin is specific, and different β spectrins and ankyrins cannot substitute for one another (Mohler et al., 2002; Ogawa et al., 2006).

βIV spectrin cannot direct ankG to the AIS

To further determine whether βIV spectrin has intrinsic localization determinants and directs ankG to the AIS, we used a mutant of AnkG-GFP (AnkG-KK-GFP) that lacks the N-terminal membrane-binding domain (that binds to Nav channels and CAMs) and the serine-rich domain, but retains the spectrin-binding domain (Fig. 3 D). Cotransfection of Myc-βIVΣ6 with AnkG-GFP or AnkG-KK-GFP permitted GFP antibodies to coimmunoprecipitate Myc-βIVΣ6, indicating that the AnkG-KK-GFP protein interacts with Myc-βIVΣ6, but GFP alone does not (Fig. 3 E). We introduced AnkG-GFP and AnkG-KK-GFP into hippocampal neurons by transient transfection. Although AnkG-GFP localized at the AIS (Fig. 4 A), AnkG-KK-GFP was never found at the AIS and, instead, was distributed throughout the cell (Fig. 4 B), much like GFP alone (not depicted). Although AnkG-KK-GFP was not found at the AIS, endogenous ankG was properly located at the AIS (Fig. 4 C; AnkG-KK-GFP

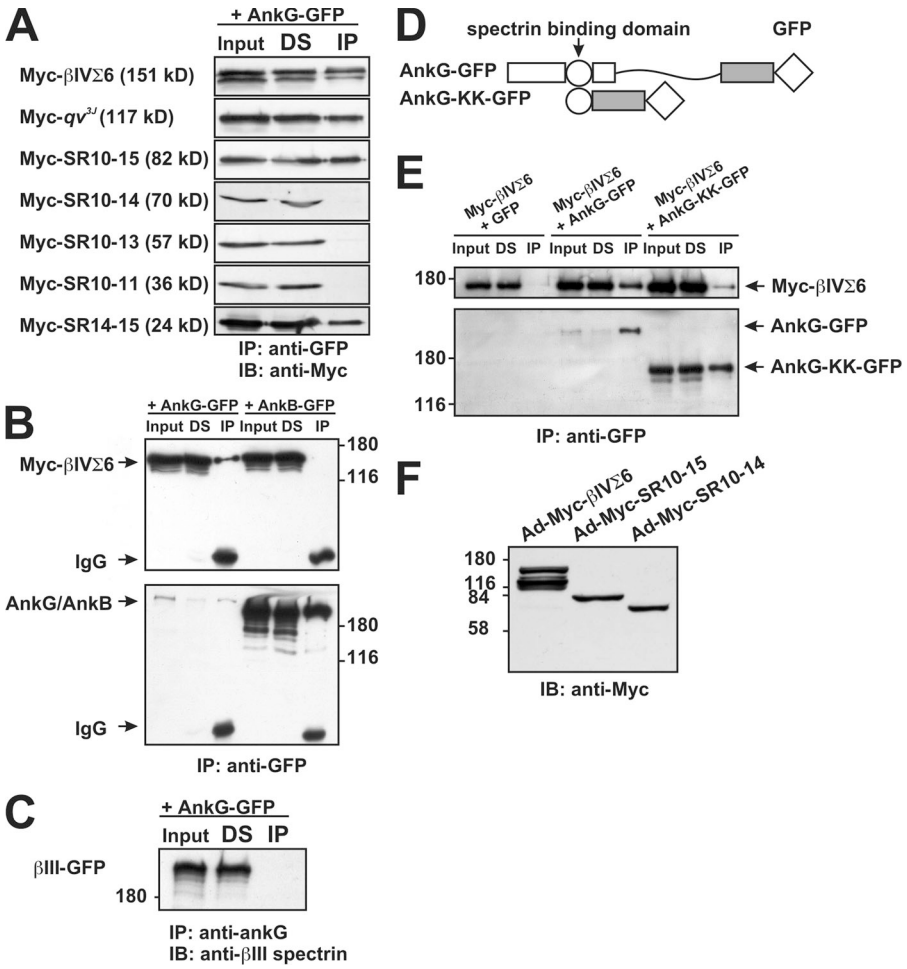

Figure 3. **SR15 in βIV spectrin binds to ankG.** (A) CHO cells were cotransfected with Myc-βIV spectrin constructs and AnkG-GFP. The soluble cell lysates were immunoprecipitated with anti-GFP antibody and immunoblotted with anti-Myc antibody. (B) COS cells were cotransfected with Myc-βIVΣ6 and AnkG-GFP or AnkB-GFP. The soluble cell lysates were immunoprecipitated with anti-GFP antibody and immunoblotted with anti-βIV spectrin or anti-GFP antibody. Starting material (Input), AnkG-GFP, or AnkB-GFP–depleted supernatants (DS), and immunoprecipitates (IP) are shown. (C) CHO cells were cotransfected with βIII spectrin-GFP and AnkG-GFP. The soluble cell lysates were immunoprecipitated with anti-ankG antibody and immunoblotted with anti-βIII spectrin. (D) Domain structure of AnkG-GFP and AnkG-KK-GFP. (E) AnkG-GFP and AnkG-KK-GFP both interact with and coimmunoprecipitate Myc-βIVΣ6 from COS cells cotransfected for the proteins. GFP alone did not interact with Myc-βIV spectrin. Soluble cell lysates were immunoprecipitated with anti-GFP antibody and immunoblotted with anti-Myc or anti-GFP antibodies. GFP signal from GFP + Myc-βIVΣ6–transfected cells could be detected at a molecular weight of ~30 kD (not depicted). (F) Anti-Myc immunoblot of CHO cells infected with adenovirus for Ad-Myc-βIVΣ6, Ad-Myc-SR10-15, and Ad-Myc-SR10-14.

lacks the epitope for anti-ankG). Transfection with AnkG-GFP did not alter the localization of either endogenous βIV spectrin (Fig. 4 D) or Nav channels (Fig. 4 F). However, transfection with AnkG-KK-GFP disrupted the localization of endogenous βIV spectrin (Fig. 4 E), indicating that this protein can act in a dominant-negative manner to disrupt βIV spectrin localization at the AIS. In contrast to the disruption of βIV spectrin, Nav channels were still located at the AIS in AnkG-KK-GFP–transfected neurons (Fig. 4 G) because Nav channels interact with the membrane-binding domain of ankG (Srinivasan et al., 1992) and this domain is not present in the AnkG-KK-GFP mutant protein. Collectively, these results show that βIV spectrin does not direct ankG or Nav channels to the AIS and supports the conclusion that βIV spectrin's AIS localization depends on ankG.

AnkG binding is required for βIV spectrin localization at the AIS in vivo

To confirm that βIV spectrin localization at the AIS in vivo also requires binding to ankG, we generated three adenoviral βIV spectrin constructs (Ad-Myc-βIVΣ6, Ad-Myc-SR10-15, and Ad-Myc-SR10-14) for expression of wild-type and mutant Myc-tagged βIV spectrins in infected neurons. Immunoblots of cell lysates from COS cells infected by these adenovirus showed that the proteins are expressed at the expected molecular weights (Fig. 3 F). To infect neurons, embryonic day (E) 14.5 mice received in utero intraventricular injections of the different adenovirus. Animals were born and allowed to mature for 1 wk, after which brains were collected, sectioned, and immunostained for Myc and Nav channel immunoreactivity. We found hundreds of cortical neurons with Myc-βIVΣ6 spectrin located at the AIS (Fig. 5 A). In the hippocampus, many initial segments can be detected using antibodies against Nav channels (Fig. 5 B), and Myc-βIVΣ6 could be detected at a subset of these initial segments (Fig. 5 B, arrows). As in cultured hippocampal neurons, we found that in vivo both cortical and hippocampal neurons expressing Myc-SR10-15 had Myc immunoreactivity restricted to the AIS that colocalized with Nav channel immunoreactivity (Fig. 5, C and D, arrows). However, Myc-SR10-14 could not be detected at the AIS of cortical or hippocampal neurons (Fig. 5, E and F, arrow). Thus, as in vitro, SR15 and ankG binding is required for βIV spectrin localization at the AIS in vivo.

AnkG binding is required for βIV spectrin localization at nodes of Ranvier

Do the rules governing assembly of the AIS also apply to nodes of Ranvier? Although AIS and nodes share a common molecular organization, the formation of nodes requires extrinsic interactions supplied by myelinating glia, whereas the AIS is intrinsically determined by neurons (for review see Schafer and

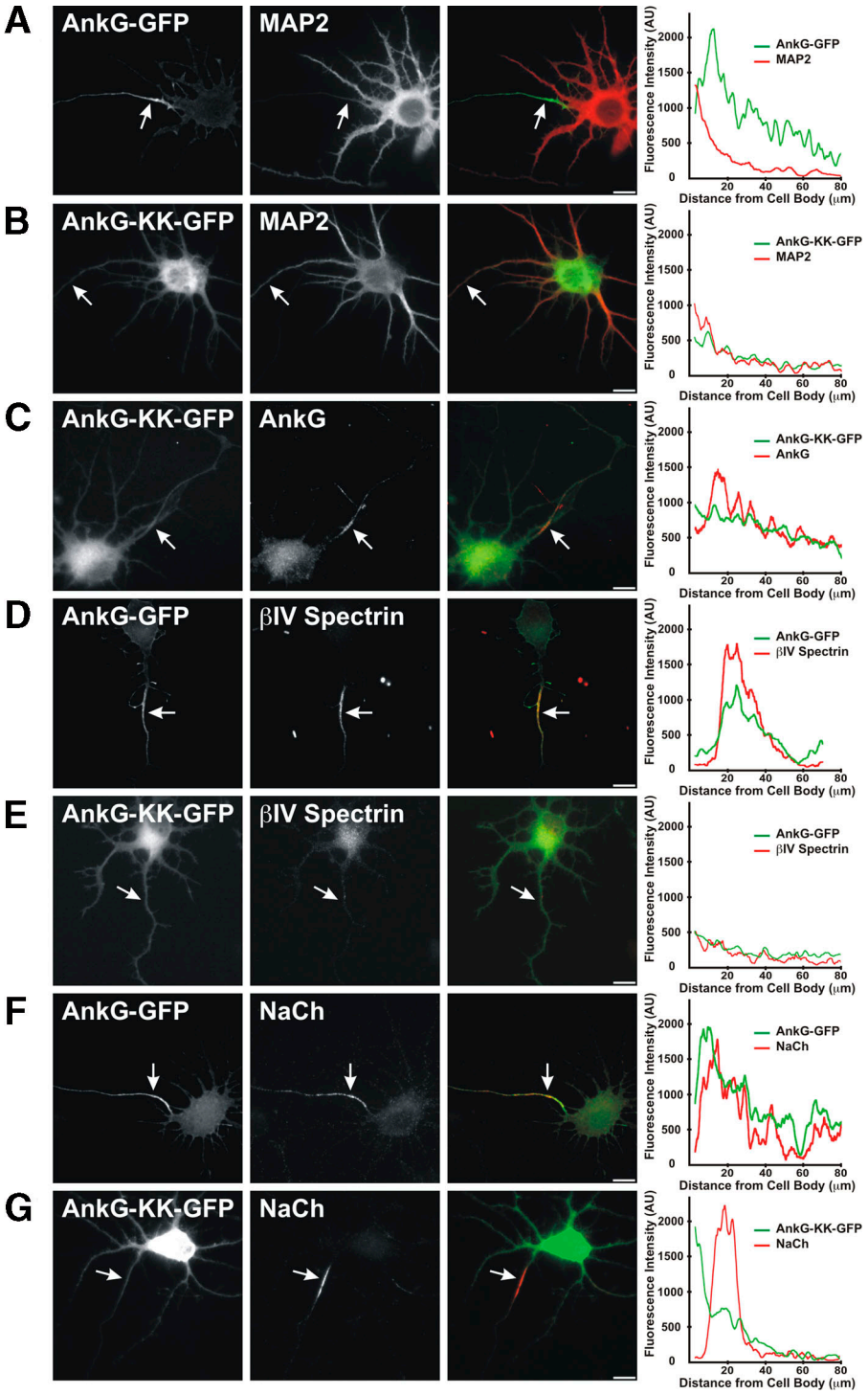

Figure 4. **AnkG directs the AIS localization of βIV spectrin.** AnkG-GFP or AnkG-KK-GFP was transfected into hippocampal neurons. (A and B) AnkG-GFP (green) is located at the AIS, but AnkG-KK-GFP is located throughout the cell. MAP2 immunostaining (red) defines the somatodendritic domain. (C) AnkG-KK-GFP (green) does not disrupt localization of endogenous ankG (red). Endogenous ankG was detected using a mouse monoclonal antibody that does not recognize AnkG-KK-GFP. (D) AnkG-GFP (green) colocalizes with endogenous βIV spectrin (red). (E) AnkG-KK-GFP (green) disrupts the localization of endogenous βIV spectrin (red). (F) AnkG-GFP (green) colocalizes with endogenous Nav channels (red). (G) In AnkG-KK-GFP–transfected (green) neurons, endogenous Nav channel (red) localization is unaffected. Axons are indicated by arrows, and fluorescence intensity profiles along the axon are shown at the right of each merged image. Bars, 10 μm.

Rasband, 2006). Nevertheless, there may be some common intrinsic mechanisms regulating both AIS and node of Ranvier formation. To determine if nodal localization of βIV spectrin depends on ankG binding, we performed intravitreal injections with Ad-Myc-βIVΣ6, Ad-Myc-SR10-15, or Ad-Myc-SR10-14 to infect adult rat retinal ganglion cells (RGCs). We collected optic nerves from the injected eyes, and we immunostained sections using anti-Myc (red) and anti-Caspr antibodies (green). Although the infection efficiency of adult RGCs was low, we could detect both Myc-βIVΣ6 and Myc-SR10-15 at many nodes of Ranvier (Fig. 6, A and B, arrows and insets). In contrast, we never detected nodal Myc immunoreactivity in Ad-Myc-SR10-14–injected mice (Fig. 6 C). Although we examined the entire optic nerve by immunostaining, we were unable to confirm that specific axons corresponded to Ad-Myc-SR10-14–infected RGC neurons because we could not detect low levels of axonal Myc immunoreactivity and we could not follow the axons of Myc-labeled RGCs from the retina into the optic nerve.

Thus, to identify myelinated axons from infected neurons and to determine if the mechanism of βIV spectrin localization

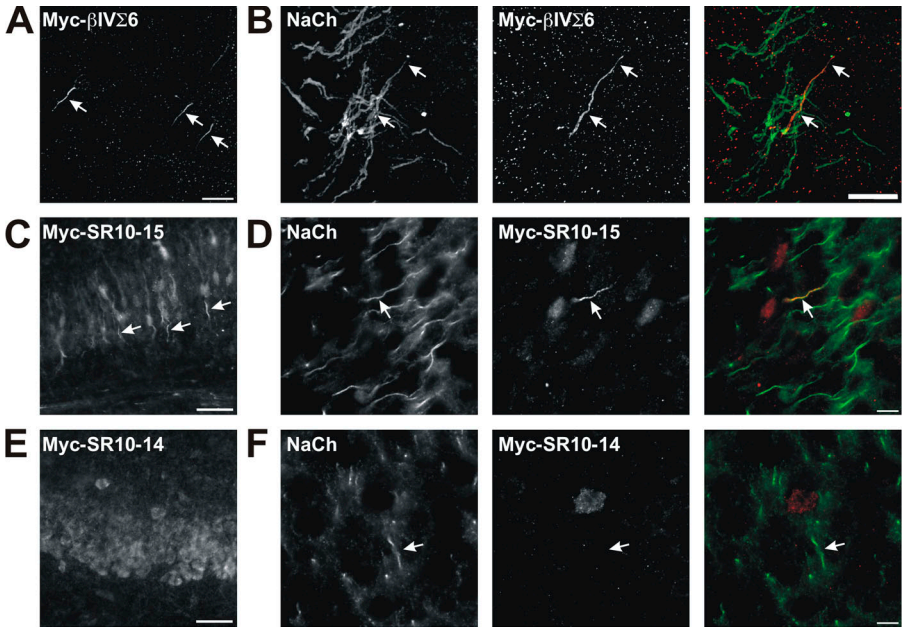

Figure 5. **βIV spectrin localization at the AIS in vivo requires binding to ankG.** (A) Cortical neurons infected by Myc-βIVΣ6 adenovirus have Myc immunoreactivity at their AIS (arrows). (B) Nav channel (NaCh; green) and Myc-βIVΣ6 immunoreactivity (red) colocalize at the AIS in hippocampus. Although many initial segments are immunostained by Nav channel antibodies, only one neuron was infected by the Myc-βIVΣ6 adenovirus and has Myc immunoreactivity at the AIS (arrows). (C) Hippocampal neurons in vivo expressing Myc-SR10-15 have Myc immunoreactivity at their AIS (arrows). (D) Nav channel (green) and Myc-SR10-15 (red) immunoreactivity colocalize at the AIS in infected mouse cortical neurons. (E) Hippocampal neurons in vivo expressing Myc-SR10-14 do not have Myc immunoreactivity at their AIS. (F) Myc-SR10-14 (red) does not localize to the AIS and does not colocalize with Nav channel immunostaining (green, arrow) in infected mouse cortical neurons. Bars: (A) 20 μm; (B, D, and F) 10 μm; (C and E) 50 μm.

to peripheral nervous system (PNS) nodes is like that of central nervous system (CNS) nodes, we used the different adenovirus to infect dorsal root ganglion (DRG) neurons in myelinated DRG-Schwann cell cocultures (Fig. 6, D–F). Very few Schwann cells were infected, but many DRG neurons were infected and could be stained using anti-Myc antibodies (Fig. 6, D–F; infected DRG neuron cell bodies are indicated by an asterisk). Nodes of Ranvier (arrows) and heminodes (arrowheads) were identified by double-immunostaining with antibodies against the paranodal protein Caspr (green), whereas Myc-βIVΣ6, Myc-SR10-15, and Myc-SR10-14 were detected using anti-Myc (red). Myc-βIVΣ6 was located at the AIS, the first heminodes (Fig. 6 D, arrowheads), and the nodes of Ranvier (Fig. 6 D, arrow and inset). Similarly, Myc-SR10-15 was located at the nodes of Ranvier (Fig. 6 E, arrows and inset). In these cultures, both Myc-βIVΣ6 and Myc-SR10-15 were detected at several hundred nodes. However, we never detected Myc-SR10-14 at any heminodes or nodes of Ranvier in myelinating DRG-Schwann cell cocultures (Fig. 6 F, arrowhead, arrow, and inset). Thus, as with the AIS, these results suggest that βIV spectrin requires SR15 for its localization to CNS and PNS nodes of Ranvier.

AnkG is properly localized at the AIS and nodes of Ranvier in βIV spectrin mutant mice

βIV spectrin is not detected at optic nerve nodes of Ranvier in qv^{3J} mutant mice, causing axonal membrane instability and dramatically widened nodes. This is in contrast to the PNS, where 40% of nodes had reduced, albeit detectable, βIV spectrin immunoreactivity (Yang et al., 2004). To confirm that ankG localization to nodes and the AIS does not require βIV spectrin, we examined ankG and Nav channel clustering in qv^{3J} mutant brain and optic nerve. In wild-type mice, ankG and Nav channels are highly enriched at nodes of Ranvier and the AIS (Fig. 7, A and D; Yang et al., 2004). Similarly, in both young and aged qv^{3J} mutant mice (qv^{3J} mutant mice usually die at ∼5–6 mo), ankG (green) is still located at broadened nodes of Ranvier (Fig. 7, B and C) and the AIS (Fig. 7, E and F). However, we did observe decreased immunoreactivity for ankG and Nav channels in the 6-mo-old mutant compared with the 1.5-mo-old qv^{3J} mutant mice (compare Fig. 7, E and F). These results show that ankG is still appropriately targeted and clustered at the AIS and nodes of Ranvier in qv^{3J} βIV spectrin mutant mice.

Discussion

Different ankyrin and spectrin isoforms are found in a variety of cell types, cytoplasmic organelles, and tissues (Bennett and Baines, 2001). Their unique spatial distributions are critical for the formation and maintenance of specific membrane domains. For example, ablation of the 190-kD isoform of ankG by RNAi disrupts lateral membrane domains in epithelial cells (Kizhatil and Bennett, 2004), and mutations in ankB disrupt the localization of the Na^+/Ca^{2+} exchanger, the Na^+/K^+-ATPase, and the inositol trisphosphate receptor in cardiomyocyte T-tubule/sarcoplasmic reticulum domains (Mohler et al., 2005). Elimination of presynaptic spectrin in *Drosophila melanogaster* results in the loss of synapse-associated CAMs and causes subsequent synapse disassembly (Pielage et al., 2005). Thus, ankyrins and spectrins function to link membrane proteins to the cytoskeleton and are indispensable for the formation and stabilization of membrane domains.

What do our results reveal about the mechanisms underlying AIS and node of Ranvier membrane domain formation? Whereas in other cellular contexts β-spectrins have been proposed to dictate ankyrin localization (De Matteis and Morrow, 1998), our results clearly demonstrate that βIV spectrin recruitment to nodes and AIS depends on binding to ankG. Consistent with this idea, βIV spectrin failed to localize properly at the AIS

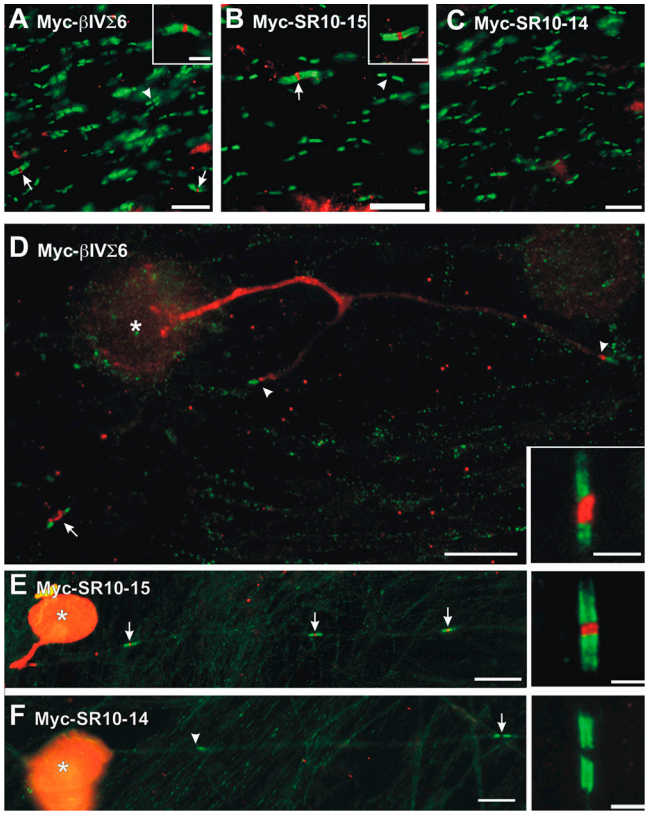

Figure 6. **βIV spectrin localization to nodes of Ranvier in the CNS requires binding to ankG.** (A–C) Adenoviruses were injected intravitreally to infect RGCs. Optic nerves were immunostained using anti-Caspr (green) and anti-Myc (red). Myc immunoreactivity was detected at nodes of neurons infected with Myc-βIVΣ6 and Myc-SR10-15 (A and B, arrows and inset), but not Myc-SR10-14 (C). Nodes of Ranvier from uninfected neurons are flanked by Caspr, but do not have Myc immunoreactivity (A and B, arrow). (D–F) Myelinated DRG-Schwann cell cocultures were infected with adenovirus to deliver the βIV spectrin transgenes indicated in each image. 4 d after infection, cocultures were fixed and immunostained using anti-Myc (red) and anti-Caspr (green) to label paranodal junctions and define nodes. Heminodes are indicated by arrowheads, nodes of Ranvier by arrows, and DRG cell bodies by an asterisk. Inset images show higher magnification of a single node of Ranvier from an infected neuron in each culture. Bars: (A–C) 10 μm; (A and B, insets) 3 μm; (D–F) 25 μm; (D–F, insets) 5 μm.

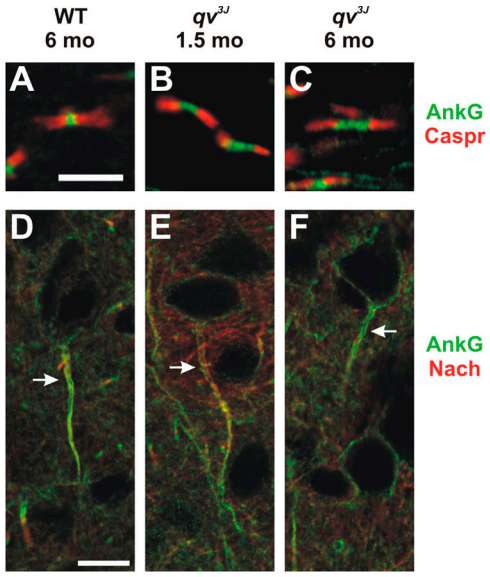

Figure 7. **AnkG is properly localized to nodes of Ranvier and AIS in qv^{3J} mutant mice.** (A–C) AnkyrinG (green) and Caspr (red) immunostaining in optic nerves of wild-type (WT) and 1.5- and 6-mo-old qv^{3J} mutant mice. (D–F) AnkG (green) and Nav channel (NaCh; red) immunostaining at the AIS (arrows) in cortex of WT and 1.5- and 6-mo-old qv^{3J} mutant mice. Bars: (A–C) 5 μm; (D–F) 10 μm.

when the dominant-negative AnkG-KK-GFP protein was expressed in neurons. Importantly, loss of βIV spectrin from the AIS did not disrupt Nav channel or endogenous ankG clustering, indicating that ankG directs βIV spectrin localization to the AIS and that βIV spectrin is not required for ankG or Nav channel clustering. This conclusion is consistent with previous studies demonstrating ankG binding is essential for the localization of many membrane proteins, including Nav channels, KCNQ2/3 Kv channels, and NF-186 at the AIS (Garrido et al., 2003; Lemaillet et al., 2003; Pan et al., 2006). Our results extend the role of ankG to clustering and localization of both cytoplasmic and membrane proteins.

Our results demonstrate that ankG directs βIV spectrin localization. However, this conclusion is in direct contrast to a recent study examining the mechanism of ankyrin and β-spectrin localization in *D. melanogaster* (Das et al., 2006). To determine the function of distinct protein domains in β spectrin, mutant forms were introduced into a fly with a lethal mutation in β spectrin. Surprisingly, loss of the putative ankyrin-binding domain (equivalent to SR15 of βIV spectrin reported in this study) had relatively little effect on localization of β spectrin, and this mutant β spectrin rescued the lethal phenotype. However, deletion of only the PH domain failed to rescue the lethal phenotype. These results suggested that the PH domain may be critical for the membrane targeting and localization of β spectrins. However, our results argue against a role for the PH domain in membrane targeting and localization of βIV spectrin because the Myc-qv^{3J} mutant βIV spectrin analyzed in this study was appropriately localized to the AIS.

If βIV spectrin is not essential for the targeting and localization of ankG and AIS formation in general, why is there a loss of ankG and Nav channels from the AIS in *βIV spectrin-null* mice (Komada and Soriano, 2002), and what is βIV spectrin's function? In this study, we examined early events in AIS formation. Previously, using mutant mice we showed that βIV spectrin is essential to maintain membrane structure and the proper molecular organization of nodes, the AIS, and the axonal cytoskeleton (Lacas-Gervais et al., 2004; Yang et al., 2004). In the analysis of *βIV spectrin-null* mice, early time points were not considered, and only initial segments of 3-mo-old mice were analyzed (Komada and Soriano, 2002). We speculate that during brain development the AIS forms properly in *βIV spectrin-null* mice, but that with increasing age the lack of βIV spectrin destabilizes this membrane domain, resulting in the loss of other AIS components. Thus, βIV spectrin is important for node and AIS stability rather than formation. Consistent with this interpretation, compared with 1.5-mo-old qv^{3J} mutant mice, there were decreased amounts of Nav channels and ankG at the AIS in 6-mo-old mutant mice.

If ankG is the central mediator of AIS and node formation, what determines its localization to these sites? In the PNS, trans-interactions between the CAMs NF-186 in axons and gliomedin on Schwann cells causes NF-186 to accumulate at the edges of myelinating Schwann cells (Eshed et al., 2005; Sherman et al., 2005). These aggregates of NF-186 are the first axonal proteins detected at nascent nodes (Lambert et al., 1997; Schafer et al., 2006). NF-186 binds to ankG, and mice lacking NF-186 fail to cluster ankG at putative nodes of Ranvier, indicating that NF-186 functions as a membrane attachment point for ankG recruitment and clustering (Tuvia et al., 1997; Sherman et al., 2005). AnkG is thought to act as a protein scaffold to retain Nav and KCNQ2/3 Kv channels at nodes (Garrido et al., 2003; Lemaillet et al., 2003; Pan et al., 2006). Our results demonstrating that SR15 and ankG binding are required for localization of βIVΣ6 spectrin to nodes of Ranvier provides the first direct evidence that ankG plays a central role in organizing the nodal protein complex. Thus, at nodes of Ranvier, extrinsic glial-derived signals regulate the eventual clustering of ankG and the subsequent accumulation of βIV spectrin.

In our experiments, we demonstrated that SR15 is necessary for βIVΣ6 localization at the AIS and nodes of Ranvier. However, we cannot rule out the possibility that additional N-terminal domains may contribute to the localization of βIVΣ1 in neurons. We consider this unlikely at the AIS because the AnkG-KK-GFP protein could block the proper localization of βIVΣ1 (both βIVΣ1 and βIVΣ6 are detected by the antibodies used in this study). However, Eshed et al. (2005) showed that the addition of a soluble fusion protein (the ectodomain of the CAM IgSF4) to cultured DRG neurons caused clustering of βIV spectrin in the absence of any colocalized ankG. Although the mechanism responsible for this clustering is unknown, this observation suggests that in the PNS additional extrinsic factors may contribute to the localization of βIVΣ1.

In contrast to nodes, much less is known about the mechanisms regulating recruitment of ankG to the AIS. Although one report indicated that multiple protein domains are required for ankG's proper AIS localization (Zhang and Bennett, 1998), the specific protein–protein interactions involved are unknown. Intriguingly, when Nav channels are eliminated from motor neurons using RNAi, ankG could not be detected at the AIS, suggesting that Nav channels, or their β subunits, may participate in ankG targeting, retention, and/or stabilization (Malhotra et al., 2002; Xu and Shrager, 2005). Thus, although the AIS and nodes of Ranvier share a common ankG-based mechanism for membrane domain formation and recruitment of βIV spectrin, the intrinsic determinants regulating ankG localization and restriction to the AIS remain unknown. Identification of the molecular mechanisms regulating ankG localization at the AIS will require a more complete description of the ankG-interacting proteins located within this membrane domain.

Materials and methods

DNA constructs, mutagenesis, and adenovirus

The full-length βIVΣ6 spectrin with N-terminal Myc tag was provided by M. Komada (Tokyo Institute of Technology, Tokyo, Japan). The C terminus deletion mutants were generated by introducing premature stop codons using the QuickChange mutagenesis kit (Stratagene) and were verified by sequencing. The following primers were used: *qv*^{3J} (aa 1–943), forward, 5′-CGGACACCCCTTGGGACTCCGGC-3′, and reverse, 5′-GCCGGAGTCCCAAGGGGTGTCCG-3′; SR10-15 (aa 1–625), forward, 5′-GCTTCCACAGCTAGGCCCGCGACC-3′, and reverse, 5′-GGTCGCGGGCCTAGCTGTGGAAGC-3′; SR10-14 (aa 1–514), forward, 5′-TCTCGGGAGCTGCATTAGTTCTTCAGCGATGC-3′, and reverse, 5′-GCATCGCTGAAGAACTAATGCAGCTCCCGAGA-3′; SR10-13 (aa 1–401), forward, 5′-GTGAGCCTGGAACAGTAGTACTGGCTCTACCAG-3′, and reverse, 5′-CTGGTAGAGCCAGTACTACTGTTCCAGGCTCAC-3′; and SR10-11(aa 1–191), forward, 5′-CCGCTTGTTGCTGGCATAAAAGGAGCTGCATCAGG-3′, and reverse, 5′-CCTGATGCAGCTCCTTTTATGCCAGCAACAAGCGG-3′. SR14-15 (aa 399–610) was amplified by PCR from pCS3 + MTβIVΣ6 plasmid and inserted into the pCS3 + MT vector (a gift from D. Turner, University of Michigan, Ann Arbor, MI) using EcoRI and XbaI sites. The primers for amplifying SR14-15 are forward, 5′-GCCGAATTCACTGGAACAGCAGTACTGGCTC-3′, and reverse, 5′-CCGTCTAGATTACGAGCATCTTCACAGGCTGCT-3′. The number of amino acid residues is based on the βIVΣ6-A (*Mus musculus*; National Center for Biotechnology Information database accession no. BAB83244). The full-length rat 270-kD ankG with C-terminal GFP tag (AnkG-GFP) and mutant ankG construct (AnkG-KK-GFP) were gifts from V. Bennett (Duke University, Durham, NC). The βIII-spectrin-GFP construct was a gift from M. Stankewich (Yale University, Stamford, CT). For adenoviral constructs, the cDNA encoding Myc-βIVΣ6, Myc-SR10-15, and Myc-SR10-14 with pEF-1α promoter was inserted into pENTR11 vector. The pENTR11 plasmids were recombined with pAd vector using ViraPower Adenoviral Gateway Expression kit (Invitrogen). Adenovirus was produced using human embryonic kidney 293 cells.

Neuronal culture and transfection

Hippocampal neurons were dissected and dissociated from E18 rat embryos, plated on 1 mg/ml poly-D-lysine (Sigma-Aldrich)/20 μg/ml laminin (Invitrogen)–coated glass coverslips at a density of 48,000 cells/cm^2. 3 h after plating, the medium was changed from normal medium (10% FBS in Neurobasal) to maintaining medium (2% B27 [Invitrogen], 0.5 mM L-glutamine, 25 μM L-glutamate, and 1× antibiotic antimycotic solution (Sigma-Aldrich) in Neurobasal). 2 d after plating, 1 μM cytosine arabinoside (Sigma-Aldrich) was added to inhibit nonneuronal growth. Half of the medium was replaced with an equal volume of maintaining medium without glutamate every 4 d. 7 d after plating, neurons were transfected with various cDNA constructs using Lipofectamine 2000 (Invitrogen) following the manufacturer's instructions. DNA/lipofectamine ratio was 1:3–4 (0.5–1 μg/1.5–4 μl for 35-mm dishes).

DRG-Schwann cell cocultures. Primary myelinating DRG-Schwann cell cocultures were prepared as in Svenningsen et al. (2003), with only minor alterations. In brief, DRG were dissected from E16 Wistar rats and collected in HBSS without calcium and magnesium (Invitrogen). Cells were mechanically dissociated after 15 min trypsin (0.25% in HBSS; Invitrogen) digestion at 37°C. Trypsinization was stopped by adding 10% FBS (Invitrogen) in Neurobasal medium (Invitrogen). Cells were centrifuged, washed, and resuspended in growth medium (Neurobasal; 2% B27), penicillin/streptomycin (Invitrogen), Glutamax (Invitrogen), and 100 ng/ml 7S NGF (Invitrogen). Cells were plated at a density of 230 cells/mm^2 on Permanox slides (Nalge Nunc International) coated with 0.4 mg/ml Matrigel (BD Biosciences)/10 μg/ml poly-L-lysine (Invitrogen). Cells were maintained and myelinated with 50 μg/ml ascorbic acid (wt/vol; Sigma-Aldrich). Myelinating cocultures (>2 wk after addition of ascorbic acid) were infected by adding adenovirus supernatants. Adenovirus was incubated for 4 h with DRG neurons; the media was then exchanged and cocultures were incubated for 4 d. Immunostaining was performed as described in Immunocytochemistry and antibodies.

Intraventricular and intravitreal injection of adenovirus. All animal procedures were performed in accordance with the National Institutes of Health guidelines for the humane treatment of animals. All procedures were approved by the Institutional Animal Care and Use Committee at the University of Connecticut Health Center. Intraventricular injection of adenovirus into embryonic mice was performed as in Tamamaki et al. (2001). Pregnant mice (E14) were deeply anesthetized. The abdominal skin was cleaned, the fur was removed, and the uterine horns were exposed. Once embryos were exposed, the adenovirus (2×10^6–10^8 pfu/ml) was injected into one side of the lateral ventricle of the mouse embryo brain using a glass micropipette and monitored by the detection of dye in the ventricles. All embryos were injected in each pregnant mouse. The uterus was placed back into the abdominal cavity and the abdomen sutured shut to allow embryonic development to continue. Injected mice were born and allowed to

develop 1–4 wk before being killed. Brains were fixed, sectioned, and stained (Schafer et al., 2004).

In the case of intravitreal injections, adult rats were anesthetized and a small incision was made in the conjunctiva around the eye. The eye was gently rotated, and a glass micropipette containing the adenovirus was inserted into the vitreous of the eye. The micropipette was positioned using micromanipulators. The injection of adenovirus was monitored by the detection of dye in the eye. Animals were allowed to recover for 3 d, and then killed. Optic nerves were dissected, fixed, sectioned, and stained (Schafer et al., 2004).

Immunocytochemistry and antibodies

24 h after transfection, hippocampal cultures and myelinating DRG-Schwann cell cocultures were fixed with 1 or 4% PFA, respectively (it should be noted that the 1% PFA resulted in a less well-preserved cytoskeleton labeled by MAP2, but this was necessary because antigenicity for some AIS proteins decreased with stronger fixation). Cells were then permeabilized and blocked with 0.3% Triton X-100 in 5% nonfat milk before being stained with antibodies. Brain and optic nerve sections were fixed and immunostained as described in Schafer et al. (2004). Mutant *qv*^{3J} mice were identified by PCR screening as previously described (Yang et al., 2004). The mouse monoclonal pan–Na^+ channel (NaCh) and Caspr antibodies have been previously described (Rasband et al., 1999; Rasband and Trimmer, 2001). Rabbit, mouse, and chicken anti-MAP2 antibodies were purchased from CHEMICON International, Inc., Sigma-Aldrich, and Encor Biotechnology, Inc., respectively. The rabbit polyclonal Nav1.6 and βIV spectrin antibodies have been previously described (Rasband et al., 2003; Ogawa et al., 2006). The mouse monoclonal ankG antibodies were purchased from Invitrogen. Rabbit polyclonal ankG antibodies were provided by V. Bennett. The Myc and βII spectrin antibodies were purchased from Sigma-Aldrich. The anti-βIII spectrin antibodies were a gift from M. Stankewich. Anti–rabbit GFP antibodies and Alexa Fluor 488– and 594–conjugated secondary antibodies to rat and mouse primary antibodies were purchased from Invitrogen. AMCA-conjugated anti–chicken secondary antibodies were purchased from Jackson Immunoresearch Laboratories.

Image acquisition and quantification

Fluorescence images were collected on an Axioskop 2 (Carl Zeiss MicroImaging, Inc.) fluorescence microscope fitted with a camera (ORCA-ER; Hamamatsu). In some cases, images were taken using an Axiovert 200M (Carl Zeiss MicroImaging, Inc.) fitted with an apotome for optical sectioning, and an axiocam digital camera. Images were taken using 63×/1.4 NA Plan-Apochromat, 40×/1.3 NA Plan-Neofluar, or 10×/0.50 NA Fluar objectives (all Carl Zeiss MicroImaging, Inc.). Acquisition software packages used included both Axiovision (Carl Zeiss MicroImaging, Inc.) and Openlab (Improvision). In some cases, stacks of images were acquired and volume reconstructions were generated using Axiovision software. In some images, contrast and brightness were subsequently adjusted using Photoshop (Adobe). No other processing of the images was performed. Exposure times were controlled so that the pixel intensity in the measured AIS was below saturation; when averages were calculated, all exposure times were held constant. Fluorescence intensity values were measured along axons by tracing a line, beginning at the cell body and running through the AIS and axon. Fluorescence values along this line were measured using ImageJ software (National Institutes of Health). MAP2 staining was used to distinguish dendrites from axons. Only neurons with an axon isolated from other cell processes were chosen for analysis. For each construct, 3–5 independent transfection experiments were done.

Immunoblotting and coimmunoprecipitation

The expression of Myc-βIVΣ6 spectrin and AnkG-GFP constructs were detected by immunoblot of cell lysates from transfected CHO or COS cells (identical results were obtained in both CHO and COS cells). The lysates were incubated on ice for 30 min and centrifuged at 13,000 *g* for 15 min at 4°C. The supernatants were denatured in SDS sample buffer, subjected to PAGE and electrophoretic transfer, and immunoblotted with Myc or GFP antibody. For coimmunoprecipitation experiments, CHO or COS cells cotransfected with spectrin constructs and ankyrin constructs were solubilized in 250 μl lysis buffer (containing 1% Triton X-100 and protease inhibitors). The soluble materials were incubated overnight with antibody and 25 μl of protein G or A agarose beads (GE Healthcare). The beads were washed six times with 1 ml lysis buffer, and then eluted with 50 μl 2× reducing sample buffer at 100°C for 5 min. The immunoprecipitates were resolved by SDS-PAGE, transferred to nitrocellulose, and subjected to immunoblotting with Myc or spectrin antibody.

Online supplemental material

Fig. S1 shows (A) the molecular weights and expression of Myc-βIVΣ6 spectrin truncation mutants expressed in CHO cells, (B–D) cultured hippocampal neurons transfected with Myc-*qv*^{3J}, Myc-SR10-13, and Myc-SR10-11, and (E) the distribution of βIII spectrin in cultured hippocampal neurons. Online supplemental material is available at http://www.jcb.org/cgi/content/full/jcb.200610128/DC1.

We thank Drs. M. Stankewich, M. Komada, V. Bennett, and J. Trimmer for helpful suggestions and/or essential reagents.

This work was supported by National Institutes of Health grant RO1 NS044916, the Patterson Trust, and a postdoctoral fellowship from the National Multiple Sclerosis Society (Y. Ogawa). M.N. Rasband was supported in part by a Harry Weaver Neuroscience Scholar award from the National Multiple Sclerosis Society.

Submitted: 27 October 2006
Accepted: 3 January 2007

References

Banker, G., and K. Goslin. 1998. Culturing Nerve Cells. The MIT Press, Cambridge. 666 pp.

Bennett, V., and A.J. Baines. 2001. Spectrin and ankyrin-based pathways: metazoan inventions for integrating cells into tissues. *Physiol. Rev.* 81:1353–1392.

Berghs, S., D. Aggujaro, R. Dirkx, E. Maksimova, P. Stabach, J.M. Hermel, J.P. Zhang, W. Philbrick, V. Slepnev, T. Ort, and M. Solimena. 2000. βIV spectrin, a new spectrin localized at axon initial segments and nodes of Ranvier in the central and peripheral nervous system. *J. Cell Biol.* 151:985–1002.

Boiko, T., A. Van Wart, J.H. Caldwell, S.R. Levinson, J.S. Trimmer, and G. Matthews. 2003. Functional specialization of the axon initial segment by isoform-specific sodium channel targeting. *J. Neurosci.* 23:2306–2313.

Chen, C., R.E. Westenbroek, X. Xu, C.A. Edwards, D.R. Sorenson, Y. Chen, D.P. McEwen, H.A. O'Malley, V. Bharucha, L.S. Meadows, et al. 2004. Mice lacking sodium channel beta1 subunits display defects in neuronal excitability, sodium channel expression, and nodal architecture. *J. Neurosci.* 24:4030–4042.

Craner, M.J., J. Newcombe, J.A. Black, C. Hartle, M.L. Cuzner, and S.G. Waxman. 2004. Molecular changes in neurons in multiple sclerosis: altered axonal expression of Nav1.2 and Nav1.6 sodium channels and Na+/Ca2+ exchanger. *Proc. Natl. Acad. Sci. USA*. 101:8168–8173.

Das, A., C. Base, S. Dhulipala, and R.R. Dubreuil. 2006. Spectrin functions upstream of ankyrin in a spectrin cytoskeleton assembly pathway. *J. Cell Biol.* 175:325–335.

Delaunay, J. 2006. The molecular basis of hereditary red cell membrane disorders. *Blood Rev*. doi:10.1016/j.blre.2006.03.005.

De Matteis, M.A., and J.S. Morrow. 1998. The role of ankyrin and spectrin in membrane transport and domain formation. *Curr. Opin. Cell Biol.* 10:542–549.

Eshed, Y., K. Feinberg, S. Poliak, H. Sabanay, O. Sarig-Nadir, I. Spiegel, J.R. Bermingham Jr., and E. Peles. 2005. Gliomedin mediates schwann cell-axon interaction and the molecular assembly of the nodes of ranvier. *Neuron*. 47:215–229.

Garrido, J.J., P. Giraud, E. Carlier, F. Fernandes, A. Moussif, M.P. Fache, D. Debanne, and B. Dargent. 2003. A targeting motif involved in sodium channel clustering at the axonal initial segment. *Science*. 300:2091–2094.

Garver, T.D., Q. Ren, S. Tuvia, and V. Bennett. 1997. Tyrosine phosphorylation at a site highly conserved in the L1 family of cell adhesion molecules abolishes ankyrin binding and increases lateral mobility of neurofascin. *J. Cell Biol.* 137:703–714.

Hedstrom, K.L., and M.N. Rasband. 2006. Intrinsic and extrinsic determinants of ion channel localization in neurons. *J. Neurochem.* 98:1345–1352.

Jenkins, S.M., and V. Bennett. 2001. Ankyrin-G coordinates assembly of the spectrin-based membrane skeleton, voltage-gated sodium channels, and L1 CAMs at Purkinje neuron initial segments. *J. Cell Biol.* 155:739–746.

Kennedy, S.P., S.L. Warren, B.G. Forget, and J.S. Morrow. 1991. Ankyrin binds to the 15th repetitive unit of erythroid and nonerythroid β-spectrin. *J. Cell Biol.* 115:267–277.

Khaliq, Z.M., and I.M. Raman. 2006. Relative contributions of axonal and somatic Na channels to action potential initiation in cerebellar Purkinje neurons. *J. Neurosci.* 26:1935–1944.

Kizhatil, K., and V. Bennett. 2004. Lateral membrane biogenesis in human bronchial epithelial cells requires 190-kDa ankyrin-G. *J. Biol. Chem.* 279:16706–16714.

Komada, M., and P. Soriano. 2002. βIV-spectrin regulates sodium channel clustering through ankyrin-G at axon initial segments and nodes of Ranvier. *J. Cell Biol.* 156:337–348.

Kordeli, E., S. Lambert, and V. Bennett. 1995. AnkyrinG. A new ankyrin gene with neural-specific isoforms localized at the axonal initial segment and node of Ranvier. *J. Biol. Chem.* 270:2352–2359.

Lacas-Gervais, S., J. Guo, N. Strenzke, E. Scarfone, M. Kolpe, M. Jahkel, P. De Camilli, T. Moser, M.N. Rasband, and M. Solimena. 2004. βIVΣ1 spectrin stabilizes the nodes of Ranvier and axon initial segments. *J. Cell Biol.* 166:983–990.

Lambert, S., J.Q. Davis, and V. Bennett. 1997. Morphogenesis of the node of Ranvier: co-clusters of ankyrin and ankyrin-binding integral proteins define early developmental intermediates. *J. Neurosci.* 17:7025–7036.

Lee, S.H., A. Simonetta, and M. Sheng. 2004. Subunit rules governing the sorting of internalized AMPA receptors in hippocampal neurons. *Neuron*. 43:221–236.

Lemaillet, G., B. Walker, and S. Lambert. 2003. Identification of a conserved ankyrin-binding motif in the family of sodium channel alpha subunits. *J. Biol. Chem.* 278:27333–27339.

Leshchyns'ka, I., V. Sytnyk, J.S. Morrow, and M. Schachner. 2003. Neural cell adhesion molecule (NCAM) association with PKCβ2 via βI spectrin is implicated in NCAM-mediated neurite outgrowth. *J. Cell Biol.* 161:625–639.

Lim, S.T., D.E. Antonucci, R.H. Scannevin, and J.S. Trimmer. 2000. A novel targeting signal for proximal clustering of the Kv2.1 K+ channel in hippocampal neurons. *Neuron*. 25:385–397.

Malhotra, J.D., M.C. Koopmann, K.A. Kazen-Gillespie, N. Fettman, M. Hortsch, and L.L. Isom. 2002. Structural requirements for interaction of sodium channel beta 1 subunits with ankyrin. *J. Biol. Chem.* 277:26681–26688.

Mohler, P.J., A.O. Gramolini, and V. Bennett. 2002. The ankyrin-B C-terminal domain determines activity of ankyrin-B/G chimeras in rescue of abnormal inositol 1,4,5-trisphosphate and ryanodine receptor distribution in ankyrin-B (−/−) neonatal cardiomyocytes. *J. Biol. Chem.* 277:10599–10607.

Mohler, P.J., J.Q. Davis, and V. Bennett. 2005. Ankyrin-B coordinates the Na/K ATPase, Na/Ca exchanger, and InsP3 receptor in a cardiac T-tubule/SR microdomain. *PLoS Biol.* 3:e423.

Naundorf, B., F. Wolf, and M. Volgushev. 2006. Unique features of action potential initiation in cortical neurons. *Nature*. 440:1060–1063.

Ogawa, Y., D.P. Schafer, I. Horresh, V. Bar, K. Hales, Y. Yang, K. Susuki, E. Peles, M.C. Stankewich, and M.N. Rasband. 2006. Spectrins and ankyrinB constitute a specialized paranodal cytoskeleton. *J. Neurosci.* 26:5230–5239.

Pan, Z., T. Kao, Z. Horvath, J. Lemos, J.-Y. Sul, S.D. Cranstoun, M.V. Bennett, S.S. Scherer, and E.C. Cooper. 2006. A common ankyrin-G-based mechanism retains KCNQ and Nav channels at electrically active domains of the axon. *J. Neurosci.* 26:2599–2613.

Parkinson, N.J., C.L. Olsson, J.L. Hallows, J. McKee-Johnson, B.P. Keogh, K. Noben-Trauth, S.G. Kujawa, and B.L. Tempel. 2001. Mutant beta-spectrin 4 causes auditory and motor neuropathies in quivering mice. *Nat. Genet.* 29:61–65.

Pielage, J., R.D. Fetter, and G.W. Davis. 2005. Presynaptic spectrin is essential for synapse stabilization. *Curr. Biol.* 15:918–928.

Poliak, S., and E. Peles. 2003. The local differentiation of myelinated axons at nodes of Ranvier. *Nat. Rev. Neurosci.* 4:968–980.

Rasband, M.N., and J.S. Trimmer. 2001. Subunit composition and novel localization of K+ channels in spinal cord. *J. Comp. Neurol.* 429:166–176.

Rasband, M.N., E. Peles, J.S. Trimmer, S.R. Levinson, S.E. Lux, and P. Shrager. 1999. Dependence of nodal sodium channel clustering on paranodal axoglial contact in the developing CNS. *J. Neurosci.* 19:7516–7528.

Rasband, M.N., T. Kagawa, E.W. Park, K. Ikenaka, and J.S. Trimmer. 2003. Dysregulation of axonal sodium channel isoforms after adult-onset chronic demyelination. *J. Neurosci. Res.* 73:465–470.

Salzer, J.L. 2003. Polarized domains of myelinated axons. *Neuron*. 40:297–318.

Sampo, B., S. Kaech, S. Kunz, and G. Banker. 2003. Two distinct mechanisms target membrane proteins to the axonal surface. *Neuron*. 37:611–624.

Sasaki, M., J.A. Black, K.L. Lankford, H.A. Tokuno, S.G. Waxman, and J.D. Kocsis. 2006. Molecular reconstruction of nodes of Ranvier after remyelination by transplanted olfactory ensheathing cells in the demyelinated spinal cord. *J. Neurosci.* 26:1803–1812.

Schafer, D.P., and M.N. Rasband. 2006. Glial regulation of the axonal membrane at nodes of Ranvier. *Curr. Opin. Neurobiol.* 16:508–514.

Schafer, D.P., R. Bansal, K.L. Hedstrom, S.E. Pfeiffer, and M.N. Rasband. 2004. Does paranode formation and maintenance require partitioning of neurofascin 155 into lipid rafts? *J. Neurosci.* 24:3176–3185.

Schafer, D.P., A.W. Custer, P. Shrager, and M.N. Rasband. 2006. Early events in node of Ranvier formation during myelination and remyelination in the PNS. *Neuron. Glia. Biol*. 2:69–79.

Sherman, D.L., S. Tait, S. Melrose, R. Johnson, B. Zonta, F.A. Court, W.B. Macklin, S. Meek, A.J. Smith, D.F. Cottrell, and P.J. Brophy. 2005. Neurofascins are required to establish axonal domains for saltatory conduction. *Neuron*. 48:737–742.

Silverman, M.A., S. Kaech, M. Jareb, M.A. Burack, L. Vogt, P. Sonderegger, and G. Banker. 2001. Sorting and directed transport of membrane proteins during development of hippocampal neurons in culture. *Proc. Natl. Acad. Sci. USA*. 98:7051–7057.

Srinivasan, Y., M. Lewallen, and K.J. Angelides. 1992. Mapping the binding site on ankyrin for the voltage-dependent sodium channel from brain. *J. Biol. Chem.* 267:7483–7489.

Svenningsen, A.F., W.S. Shan, D.R. Colman, and L. Pedraza. 2003. Rapid method for culturing embryonic neuron-glial cell cocultures. *J. Neurosci. Res.* 72:565–573.

Tamamaki, N., K. Nakamura, K. Okamoto, and T. Kaneko. 2001. Radial glia is a progenitor of neocortical neurons in the developing cerebral cortex. *Neurosci. Res.* 41:51–60.

Tuvia, S., T.D. Garver, and V. Bennett. 1997. The phosphorylation state of the FIGQY tyrosine of neurofascin determines ankyrin-binding activity and patterns of cell segregation. *Proc. Natl. Acad. Sci. USA*. 94:12957–12962.

Winckler, B., P. Forscher, and I. Mellman. 1999. A diffusion barrier maintains distribution of membrane proteins in polarized neurons. *Nature*. 397:698–701.

Wisco, D., E.D. Anderson, M.C. Chang, C. Norden, T. Boiko, H. Folsch, and B. Winckler. 2003. Uncovering multiple axonal targeting pathways in hippocampal neurons. *J. Cell Biol.* 162:1317–1328.

Xu, X., and P. Shrager. 2005. Dependence of axon initial segment formation on Na+ channel expression. *J. Neurosci. Res.* 79:428–441.

Yang, Y., S. Lacas-Gervais, D.K. Morest, M. Solimena, and M.N. Rasband. 2004. BetaIV spectrins are essential for membrane stability and the molecular organization of nodes of Ranvier. *J. Neurosci.* 24:7230–7240.

Zhang, X., and V. Bennett. 1998. Restriction of 480/270-kD ankyrin $_G$ to axon proximal segments requires multiple ankyrin G-specific domains. *J. Cell Biol.* 142:1571–1581.

Zhou, D., S. Lambert, P.L. Malen, S. Carpenter, L.M. Boland, and V. Bennett. 1998. AnkyrinG is required for clustering of voltage-gated Na channels at axon initial segments and for normal action potential firing. *J. Cell Biol.* 143:1295–1304.